Applied Catalysis B: Environmental 221 (2018) 556–564

Contents lists available at ScienceDirect

Applied Catalysis B: Environmental

journal homepage: www.elsevier.com/locate/apcatb

De-reducibility mechanism of titanium on maghemite catalysts for the SCR reaction: An *in situ* DRIFTS and quantitative kinetics study

Dong Wang[a,b], Yue Peng[a,*], Shang-chao Xiong[a], Bing Li[a], Li-na Gan[a], Chun-mei Lu[b], Jian-jun Chen[a], Yong-liang Ma[a], Jun-hua Li[a,*]

[a] State Key Joint Laboratory of Environment Simulation and Pollution Control, School of Environment, Tsinghua University, Beijing 100084, China
[b] National Engineering Laboratory for Coal-Burning Pollutants Emission Reduction, School of Energy and Power Engineering, Shandong University, Jinan 250061, China

ARTICLE INFO

Keywords:
NO_x
SCR
Maghemite
DRIFTS
Kinetic

ABSTRACT

An environmental benign TiO_2 doped maghemite catalyst, the γ-$Fe_{95}Ti_5$, was prepared via the precipitation microwave pyrolysis method for the NO_x removal. The γ-$Fe_{95}Ti_5$ exhibited significantly higher catalytic activity and better N_2 selectivity than the pure maghemite, γ-$Fe_{100}Ti_0$. The SCR active window of the catalyst is broadened and the resistances to H_2O and SO_2 are also preserved. Ti^{4+} cations could enter the lattice of γ-$Fe_{100}Ti_0$, forming the partial solid solution on the catalyst surface, as γ-$Fe_{2-\zeta}Ti_{\zeta}O_{3+\xi}$. This structure improves the quantity and stability of both Lewis and Brönsted acid sites compared with the γ-$Fe_{100}Ti_0$. Meanwhile, the dopant cations suppress the reduction of Fe^{3+} and the percentage of active oxygen on the catalyst surface. These could suppress the N_2O formation from NH_3 oxidation and NO_x reduction. By the combination of both DRIFTS and kinetic methods, the rate constants of the γ-$Fe_{95}Ti_5$ catalyst via the Eley-Rideal and Langmuir-Hinshelwood mechanisms increase simultaneously, while the rate constant via the catalytic oxidation of NH_3 decreases compared with the γ-$Fe_{100}Ti_0$.

1. Introduction

The removal of NO_x has attracted the world-wide attentions due to the serious threat to human health and environment [1–3]. The selective catalytic reduction (SCR) of NO_x by NH_3 is one of the most efficient methods that has been widely applied in coal-fired power plant. Commercial V_2O_5-WO_3(MoO_3)/TiO_2 catalyst exhibits high activity at standard working temperatures (350–420 °C) [4–6]. However, there are still some inevitable disadvantages, such as the toxicity of V_2O_5 and secondary pollution caused by fly ash at high temperatures [7]. Furthermore, the relative narrow active window restricts its utilization in the industry boilers and waste incineration. Thus, it is necessary to develop the SCR catalyst with high activity in a wider temperature window.

A series of transitional and rare-earth metals have been adopted as active components and/or additions during the catalyst design because of their appropriate reducibility and surface acidity [8–13]. Iron exhibits great potentials for the SCR catalyst due to its accessibility and good activity. Maghemite, as a non-stoichiometric iron oxide, was used in catalytic oxidation for its excellent reducibility and oxygen storage-release ability. It can be considered as an Fe(II)-deficient magnetite with formula $(Fe_8^{III})_A[Fe_{40/3\circ 8/3}^{III}]_BO_{32}$ where ○ represents a cations vacancy, A and B indicates tetrahedral and octahedral positioning respectively. Part of Fe^{3+} (convert from Fe^{2+} in magnetite) are metastable, which are easily reduced to Fe^{2+} [14,15]. However, it was not an appropriate iron-based catalyst for the SCR reaction due to its excessive reducibility and unstable surface acidity. Therefore, many researchers tried to modify the stability and acidity of this catalyst by cations doping method.

The stability of metastable iron cations can be improved by depressing the electronegativity around them. Donor dopants (dopants with higher valence) can decrease the electronegativity around cations and enrich cation vacancies simultaneously [16,17]. It is predictable that when higher valence ions with larger ionic radius are incorporated into the lattice, at least two positive effects will be produced: (1) increasing the stability of adjacent ions; (2) emerging more cation vacancies. Titanium is a perfect donor dopants and has a high valence stability in the SCR reaction. Moreover, Ti^{4+} cations exhibit great surface acidity and are independent of the redox cycle. The ionic radius of 6 coordinated Ti^{4+} (0.745 Å) is close to that of Fe^{3+} (0.69 Å). Thus, Ti^{4+} is supposed to be a good dopant for balance the reducibility and surface acidity of maghemite.

Kinetic study is an important way to guide the design of catalysts. However, there is still a lack of rigorous demonstration for the exact path of the SCR reaction over maghemite [18,19]. The quantitative

* Corresponding authors.
E-mail addresses: pengyue83@tsinghua.edu.cn (Y. Peng), lijunhua@tsinghua.edu.cn (J.-h. Li).

http://dx.doi.org/10.1016/j.apcatb.2017.09.045
Received 12 June 2017; Received in revised form 19 August 2017; Accepted 19 September 2017
Available online 22 September 2017
0926-3373/

studies should solve the contributions, rate-determining steps and key factors of the Eley-Rideal mechanism (E-R mechanism, adsorbed NH_3 reacts with gaseous NO), Langmuir-Hinshelwood mechanism (L-H mechanism, adsorbed NH_3 reacts with adsorbed NO), and Catalytic-Oxidation reaction (C-O reaction). Nevertheless, the C-O reaction was not yet taken into account during the former kinetic study of NO reduction over iron-based catalysts [20–22].

This work attempts to investigate the SCR performance and intrinsic properties over maghemite catalysts. The novel γ-$Fe_{95}Ti_5$ catalyst has high SCR activity, N_2 selectivity, thermal stability and H_2O/SO_2 durability. A global quantitative kinetic study over maghemite catalysts was studied by the steady-state kinetic experiments.

2. Experimental

2.1. Catalyst preperation

Maghemite catalysts were prepared via precipitation microwave pyrolysis method using $FeSO_4{\cdot}7H_2O$ and $Ti(SO_4)_2$. NH_4OH was used as precipitator. The precursors were first dissolved into deionized water, in which the total concentration of cation was 0.1–0.5 mol·L^{-1}. The mixed solution was stirred at 20 °C for 1 h. Then, NH_4OH was introduced into the mixed solution until the pH of the solution reached 9–10. Without aging, the precipitate was filtered washing with deionized water for certain times, followed by heat treatment with microwave assisted. After that, the precipitate was desiccated at 105 °C for 12 h and then calcined at 375–425 °C for 5 h under air atmosphere. The calcined samples were crushed and sieved to a size of 40–60 mesh for catalytic activity test. The maghemite catalysts were denoted as the γ-$Fe_{100}Ti_0$ and γ-$Fe_{95}Ti_5$, where the number represents the mole percent of the corresponding elements.

2.2. Catalyst characterization

The crystalline phase of catalysts was measured by powder X-ray diffraction (XRD) using a Rigaku D/MAC/max 2500 v/pc diffractometer (Japan, Cu K_α as radiation resource, λ = 0.15406 nm) with a nickel filter operating at 50 kV and 150 mA in the 2θ range of 10–90° at a scanning rate of 4°·min^{-1}. The diffraction lines were identified by matching with reference patterns in the JCPDS database.

N_2 adsorption-desorption isotherms over maghemite catalysts were obtained at −196 °C using Micromeritics ASAP2020 Surface Area and Porosity Analyzer. Prior to N_2 physisorption, the catalysts were degassed at 300 °C for 5 h. Average pore diameters, pore volumes and pore size distributions were determined by Barrett-Joyner-Halenda (BJH) method from the desorption branches of the isotherms. Surface areas were determined by Brunauer-Emmertt-Teller (BET) equation in 0.05–0.35 partial pressure range. Textural properties of micropores were calculated using t-plot model.

The chemical states of surface compositions were observed by X-ray photoelectron spectra (XPS) recorded using a Kratos' Axis Ultra DLD photoelectron spectrometer. Wide spectrum test conditions were Pass energy: 160 eV, Anode: Mono (Al, 112 W), Step (meV): 1000.0, Dwell Time (ms): 150. Fine spectrum test conditions were Pass energy: 40 eV, Anode: Mono (Al, 112 W), Step (meV): 100.0, Dwell Time (ms): 600. Binding energies were calibrated using C 1 s (BE = 184.8 eV) as a standard.

The thermal stability of maghemite catalysts was analyzed utilizing thermogravimetric-derivative thermogravimetric (TG-DTG) recorded on a TGA/SDTA 851e (Mettler-Toledo, Co., Ltd, Switzerland). The samples were weighted to 10 ± 0.1 mg in an aluminum oxide ceramic crucible with depth of 5 mm and inner diameter of 5 mm, and heated from 25 °C to 325 °C at 10 °C·min^{-1} under N_2 flow (with the concentration of 99.99%) of 40 mL·min^{-1}. The protection gas is 30 mL·min^{-1} of N_2, with the concentration of 99.99%.

Hydrogen-temperature programmed reduction (H_2-TPR) was carried out on a Micromeritics' Chemisorb 2720 TPx Chemisorption Analyzer calibrated using Ag_2O. The catalyst samples (30–40 mg) were pretreated at 500 °C for 30 min in Ar gas (50 mL·min^{-1}) and then cooled down to 50 °C. The measurement was carried out at the temperature range of 50 − 1100 °C, in the steam of 10 vol.% H_2/Ar, with a heating rate of 10 °C·min^{-1}.

Temperature programmed desorption of ammonia (NH_3-TPD) was performed on the chemisorption analyzer of Micromeritics' AutoChem 2920. The catalyst samples (90 mg) were first pretreated at 300 °C for 1 h in Ar gas and then cooled down to 50 °C. After that, the samples were exposed to 10 vol.% NH_3/He for 30 min at 50 °C, followed by Ar purge for another 1 h at 100 °C. Finally, the temperature programed desorption was run to 700 °C in Ar flow with heating rate of 5 °C·min^{-1}.

In situ DRIFT spectra were recorded on a Fourier Transform Infrared Spectrometer (FTIR, Nicolet NEXUS 870) equipped with a liquid-nitrogen-cooled MCT detector, collecting 100 scans with a resolution of 4 cm^{-1}.

2.3. Catalyst acticity measurement

The SCR activity over the maghemite catalysts were measured in a fixed-bed quartz reactor. The test was carried out under atmospheric pressure at the temperature range of 100–350 °C. The total flow rate was 200 mL·min^{-1} responding to the GHSV of 60,000·mL·g^{-1}·h^{-1}. The typical reactant gas composition was as follows: 500 ppm NH_3, 500 ppm NO, 3 vol.% O_2, 200–800 ppm SO_2 (when used), 5/10 vol.% H_2O (when used) and balance N_2. The concentrations of the gases (NO, NO_2, N_2O, and NH_3) were continually monitored by an FTIR spectrometer (MultiGas TM 2030 FTIR Continuous Gas Analyzer). And the data was recorded only when the SCR reaction reached the steady state after 30 minutes of continuous and stable operation running at each measuring temperature. As the SCR reaction reached the steady state, the ratio of NO_x conversion (η), N_2O selectivity (S) and the pseudo-first order rate constant (τ) of the SCR reaction were calculated according to the following equations:

$$\eta = \frac{[NO_x]_{in} - [NO_x]_{out}}{[NO_x]_{in}} \times 100\% \quad (1)$$

$$S = \frac{2[N_2O]_{out}}{[NH_3]_{in} + [NO_x]_{in} - [NH_3]_{out} - [NO_x]_{out}} \times 100\% \quad (2)$$

$$\tau = -\frac{V}{W} \times \ln(1 - \eta) \quad (3)$$

where $[NO_x]_{in}$ and $[NO_x]_{out}$ were the concentrations of gaseous NO_x in the inlet and outlet, respectively; $[N_2O]_{out}$ was the concentration of gaseous N_2O in the outlet; V was the total flow rate; and W was the mass of catalyst (g).

3. Results and discussion

3.1. SCR performance

3.1.1. SCR activity

Fig. 1 shows that doping of 5% titanium has a considerable impact on the NH_3-SCR reaction over maghemite catalyst. The γ-$Fe_{95}Ti_5$ showed a good SCR activity in the range of 250–300 °C (NO_x conversion was higher than 80%). Whereas the NO_x conversion of the γ-$Fe_{100}Ti_0$ was only about 40% at 250 °C, and further decreased above 300 °C. The outlet NO_x concentration of the γ-$Fe_{100}Ti_0$ was even higher than the inlet data at 350 °C (shown in Fig. 1a), and the NO_x conversion was lower than the NH_3 conversion above 300 °C. The results suggest that part of NH_3 was directly oxidized to NO with O_2 on the γ-$Fe_{100}Ti_0$ catalyst. High percentage of N_2O formed on the γ-$Fe_{100}Ti_0$ above 150 °C. In contrast, the γ-$Fe_{95}Ti_5$ catalyst showed excellent N_2 selectivity (close to 100%) in the range of 250–300 °C. Compared with the

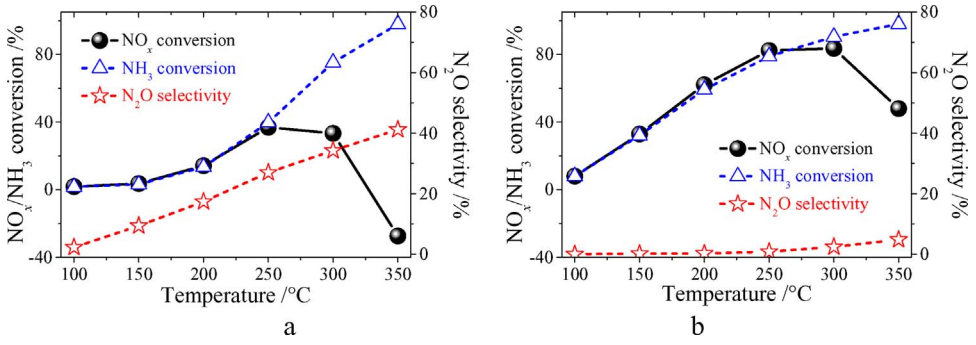

Fig. 1. SCR performance of maghemite catalysts: (a) γ-$Fe_{100}Ti_0$; (b) γ-$Fe_{95}Ti_5$. Reaction conditions: [NH_3] = [NO] = 500 ppm, [O_2] = 3%, catalyst mass = 200 mg, total flow rate = 200 mL·min^{-1}, and gas hourly space velocity (GHSV) = 60 000 cm^3·g^{-1}·h^{-1}.

excellent modified low temperature catalysts [23,24], the remarkably improved activity and selectivity of γ-$Fe_{95}Ti_5$ exhibited in the middle temperature range are much impressive. Therefore, the doping of titanium prohibits the formation of N_2O on the maghemite, leading to the improvement of N_2 selectivity and catalytic activity.

3.1.2. Effect of H_2O and SO_2

The influence of SO_2 and H_2O on the γ-$Fe_{95}Ti_5$ was investigated and shown in Fig. 2. During the first 7 h (SO_2 concentration was 200 or 400 ppm), there was no obvious activity drop on the γ-$Fe_{95}Ti_5$ and the commercial catalyst. When 600 ppm of the SO_2 were introduced, the NO_x conversion for commercial catalyst and the γ-$Fe_{95}Ti_5$ dropped by 5% and 3% respectively. When 800 ppm of the SO_2 were introduced, the activity of the commercial catalyst decreased from 100% to 80%, while the activity of the γ-$Fe_{95}Ti_5$ was only decreased from 85% to 78%. As soon as the SO_2 was shut down, the activity of the γ-$Fe_{95}Ti_5$ rapidly recovered to 83% within 10 min, while the activity of the commercial catalyst recovered to 92% relatively slow in 1 h. It can be inferred that metal sulfate formed on the surface of the commercial catalyst under the operating conditions with high sulfur concentrations, resulting in irreversible changes over the catalyst surface. In contrast, the γ-$Fe_{95}Ti_5$ catalyst performed higher and reversible poisoning resistance to SO_2 compared with the commercial catalyst.

When H_2O was introduced into the flue gas, NO_x conversion of the γ-$Fe_{95}Ti_5$ and commercial catalyst both decreased. When the 5 vol.% H_2O was removed, the NO_x conversions both recovered. After 10 vol.% H_2O was introduced for 3 h, NO_x conversion of commercial catalyst and the γ-$Fe_{95}Ti_5$ decreased to 85% and 63% respectively. As soon as H_2O was removed, NO_x conversion of the two catalysts reversed. The results indicate that the inhibition effect of H_2O could be due to the competitive adsorption of H_2O and NH_3 on acid sites. [25] It can be concluded that there was almost no hydroxyl functional group formed on the commercial catalyst and the maghemite catalyst surface, thus, no irreversible change occurred on the catalyst surface. As shown in Fig. 7 **S**, when SO_2 and H_2O were introduced into the flue gas simultaneously, NO_x conversion was comparable to that in Fig. 2b. After 780 min, SO_2 and H_2O were shut off. NO_x conversion reversed to 74%, which was lower than the initial conversion. As compared with Fig. 2, it can be concluded that H_2O was the main reason for the decrease of NO_x conversion under this reaction condition. Moreover, the catalyst had good stability and no irreversible change happened to the catalyst structure.

Table 1
The BET surface area (S_{BET}) values and the reaction rate constant.

Samples	S_{BET}/ m^2·g^{-1}	Reaction Rate Constant [a]/ cm^3·g^{-1}·s^{-1}	Reaction Rate Constant [b]/mL·m^2·s^{-1}
γ-$Fe_{100}Ti_0$	17.40	2.55	0.15
γ-$Fe_{95}Ti_5$	48.03	16.17	0.34

[a] calculated by the NO_x conversion results at 200 °C.
[b] calculated by the NO_x conversion results at 200 °C and the S_{BET} results.

3.1.3. Pore structure

The BET surface area (Table 1) and BJH desorption pore volume (Table 1**S**) of the γ-$Fe_{95}Ti_5$ were 48.03 m^2·g^{-1} and 0.21 cm^3·g^{-1}, respectively, which were nearly 3 times higher than the γ-$Fe_{100}Ti_0$. The pore volume distribution, cumulative pore volumes, and N_2 adsorption-desorption isotherms of maghemite catalysts are shown in Fig. 1**S**. The pore structure of the γ-$Fe_{95}Ti_5$ was mainly in the range of 2–150 nm, especially within 2 to 4 nm. Generally, small pores provide sufficient surface area and pore volume improving the acid sites, while large pores ensure the mass transfer process enhancing the reaction rate. Therefore, the versatile pore structures and volume distribution are both important factors for the SCR performance. The isotherm resembled closely with type V isotherm according to the IUPAC classification (Fig. 2**S**), which is typical for mesoporous materials. The hysteresis loops exhibited a shape of typical H3 type, revealing the existence of the slit-shaped pore structures in the maghemite catalysts. It can be summarized that the γ-$Fe_{95}Ti_5$ presents the pore volume

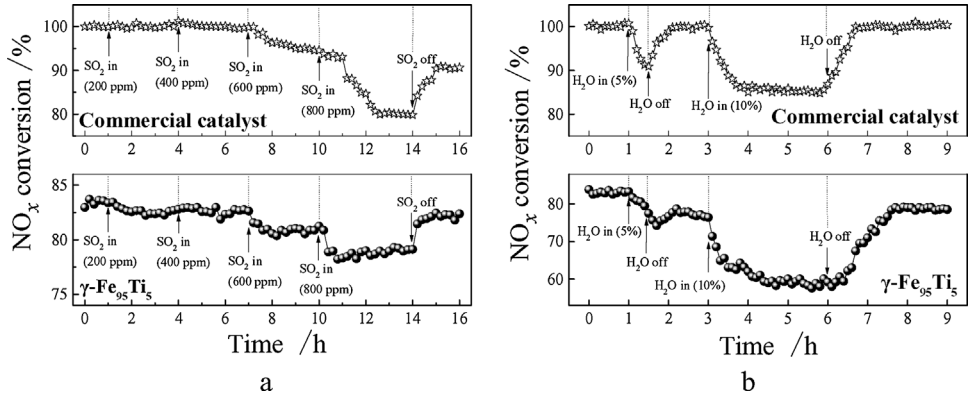

Fig. 2. (a) Effect of SO_2 on the NH_3-SCR activity of maghemite catalysts. Reaction condition: [NH_3] = [NO] = 500 ppm, [O_2] = 3%, [SO_2] = 200 – 800 ppm, reaction temperature: 300 °C, catalyst mass = 200 mg, total flow rate = 200 mL·min^{-1}; GHSV = 60 000 cm^3·g^{-1}·h^{-1}. (b) Effect of H_2O on the NH_3-SCR activity of maghemite catalysts; Reaction condition: [NH_3] = [NO] = 500 ppm, [O_2] = 3%, [H_2O] = 5/10 vol.%, reaction temperature: 300 °C, catalyst mass = 200 mg, total flow rate = 200 mL·min^{-1}; GHSV = 60 000 cm^3·g^{-1}·h^{-1}.

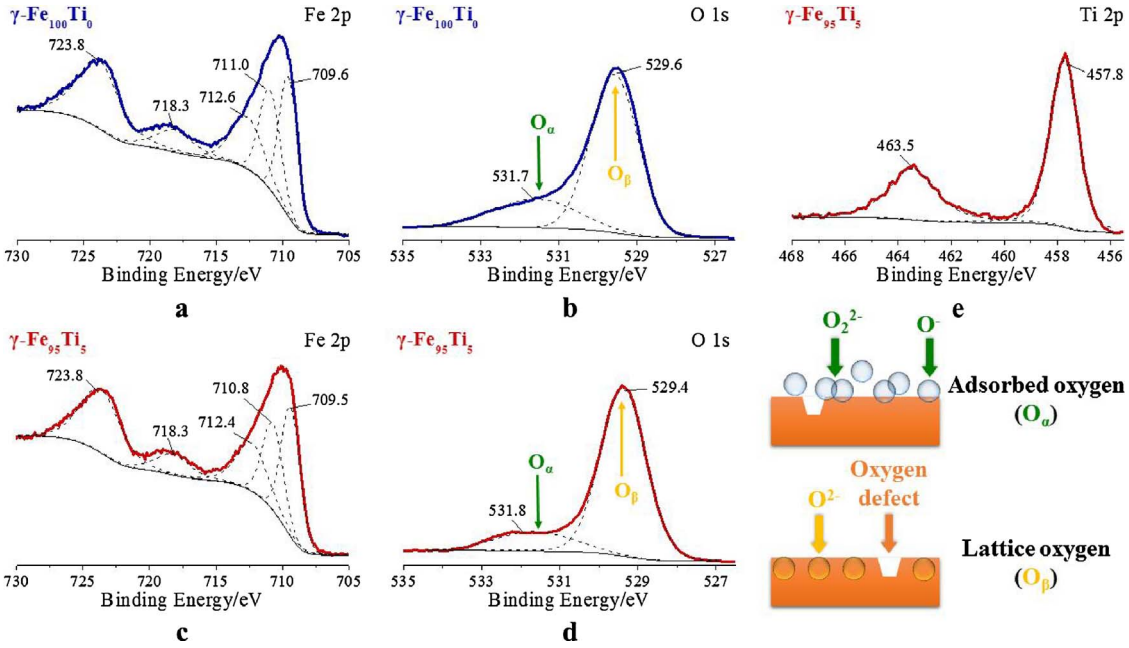

Fig. 3. XPS spectra of maghemite catalysts over the spectral regions of Fe 2p and O 1s.

distribution curve uniformly as semi-hyperbolic curves (with the decrease of pore diameter, the pore volume increases monotonically). This provides adequate amount of large pores in the γ-$Fe_{95}Ti_5$, promoting the mass transfer and diffusion, and also provides plenty of small pores for surface active sites.

The pseudo-first order rate constants based on the surface area and mass constants at 200 °C for maghemite catalysts are calculated using Eq. (3) and summarized in Table 1. The rate constants normalized by mass and surface area on the γ-$Fe_{95}Ti_5$ are 16.17 $mL{\cdot}g^{-1}{\cdot}s^{-1}$ and 0.34 $mL{\cdot}m^{2}{\cdot}s^{-1}$, respectively, which are higher than those of the γ-$Fe_{100}Ti_0$. This indicates that the notable increase of SCR activity is not just due to the pore structure, but due to its surface chemical property. Therefore, we elucidate the improvement mechanism from chemical characterizations in the following parts.

3.2. Characterization

3.2.1. Chemical state of surface composition

XPS experiments over maghemite catalysts were undertaken and the spectra were recorded, as shown in Fig. 3. XPS peaks for Fe 2p3/2 and Fe 2p1/2 are located at 709.2 eV and 723 eV, respectively. It can be concluded that the peaks at the binding energy of 709.6 eV, 709.5 eV, 711.0 eV, 710.8 eV, 712.6 eV, and 712.4 eV represent Fe 2p3/2, and that of 723.8 eV represent Fe 2p1/2 (shown in Fig. 3a and c). These 2 peaks could be assigned to the Fe^{3+} characteristic peaks, indicating that Fe^{3+} was the main form of iron over the surface of maghemite catalysts. The binding energies of Fe 2p3/2 decreased after the titanium doping. This suggests that the density of the outer electron cloud increases around Fe^{3+} cations. Thus, the electronegativity of iron cations decreases and their SCR activity are suppressed [26]. Between the 2 characteristic peaks around 709.2 eV and 723 eV, both of the maghemite catalysts shows a relatively flat and broad peaks around 718.3 eV. This is a typical feature of iron oxides rather than hydroxyl iron.

The O1 s spectra of the maghemite catalysts are shown in Fig. 3b and d. The peaks at 529.6 eV and 529.4 eV are attributed to the lattice oxygen O^{2-} of the catalyst surface, denoted as O_β. The peaks at 531.7 eV and 531.8 eV are attributed to the adsorbed oxygen, which corresponds to the O_2^{2-} caused by the surface oxygen defect, or the O^- corresponding to −OH, denoted as O_α. [27] The oxygen defects and weakly adsorbed oxygen species on the catalyst surface can improve the catalytic oxidation capacity of catalysts. The γ-$Fe_{95}Ti_5$ had more O_β than that of the γ-$Fe_{100}Ti_0$, exhibiting larger amount of surface lattice oxygen O^{2-}. This indicates that the charge imbalance of γ-$Fe_{95}Ti_5$ is mainly compensated by the lattice oxygen. The valence reducing of iron cations was minimized which guaranteed the stability of main crystalline phase. Meanwhile, the content of O_α on the γ-$Fe_{95}Ti_5$ was less than that of the γ-$Fe_{100}Ti_0$, which indicates that the surface oxygen defects decreased. The enrichment of lattice oxygen may repair partial surface oxygen defects and inhibit the catalytic oxidation capacity.

Fig. 3e showed the Ti 2p spectra of γ-$Fe_{95}Ti_5$. The XPS characteristic peak around the binding energy of 457.8 eV, corresponding to Ti 2p3/2, represents the Ti^{4+}. Therefore, the Ti was mainly in the form of Ti^{4+} over the surface of the maghemite catalyst. Ti^{4+} can promote the adsorption of oxygen molecules on the surface of the catalyst.

3.2.2. Crystalline phase

Fig. 4 shows the XRD patterns of maghemite catalysts. Both of the catalysts exhibited sharp diffraction peaks attributing to γ-Fe_2O_3

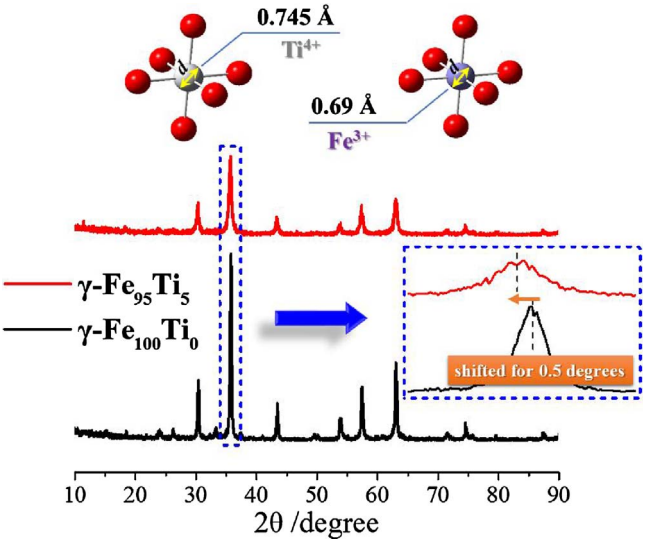

Fig. 4. XRD patterns of maghemite catalysts.

(maghemite) at 2θ = 31°, 36°, 43°, 54°, 57° and 63° (JCPDS: #39-1-346), indicating that the dominated phase of both the γ-$Fe_{100}Ti_0$ and γ-$Fe_{95}Ti_5$ is γ-Fe_2O_3. The titanium doping to γ-Fe_2O_3 will not change the characteristic structure of catalyst. The γ-$Fe_{95}Ti_5$ showed lower γ-Fe_2O_3 characteristic peak with an obvious passivation, proving that titanium is of effect on reducing the crystallite size of the maghemite catalyst. It can be observed from the amplified XRD spectra that all the characteristic peaks of the γ-$Fe_{95}Ti_5$ shifted to the left for c.a. 0.5 degrees. The results indicate that the lattice constant of γ-Fe_2O_3 become slightly larger, which is caused by interfusing metal cations which has larger ionic radius than the main cations. [28] The iron cations in γ-Fe_2O_3 are Fe^{3+} with the coordination number of 6 in metastable state (0.69 Å). The ionic radius of Ti^{4+} with the coordination number of 6 is 0.75 Å. Their ionic radius difference is only 7.4%, which is easy to form partial solid solution. Moreover, the peaks of TiO_2 were not detected in the XRD spectra. This indicates that maghemite and doped titanium formed stable partial solid solution, as γ-$Fe_{2-\zeta}Ti_\zeta O_{3+\xi}$, and the main crystal structure was not changed. 4 Fe^{3+} transferred into 3 Ti^{4+} in some parts of γ-$Fe_{2-\zeta}Ti_\zeta O_{3+\xi}$. Where, 1/4 of the positions occupied by Fe^{3+} emerged vacancies, leading to the presence of cations vacancies to maintain the electrical neutrality. [16] These cations vacancies play an important role in enriching the surface acidity of catalysts, which is favorable for SCR reaction.

3.3. Physical and chemical properties

3.3.1. Reducibility

The H_2-TPR results of the γ-$Fe_{100}Ti_0$ and γ-$Fe_{95}Ti_5$ were shown in Fig. 5a. The reduction peak of the γ-$Fe_{95}Ti_5$ shifted to higher temperature and the peak pattern changed obviously compared to the γ-$Fe_{100}Ti_0$. This indicates that titanium doping significantly change the reducibility of the catalyst. The typical reduction process of maghemite can be divided into 3 processes: $Fe_2O_3 \rightarrow Fe_3O_4 \rightarrow FeO \rightarrow Fe$. The $Fe_2O_3 \rightarrow Fe_3O_4$ process mainly occurs in the temperature range of 350 − 400 °C. The peaks at 366 °C of the γ-$Fe_{100}Ti_0$ are attributed to the reduction of $Fe_2O_3 \rightarrow Fe_3O_4$. The reduction peak of the γ-$Fe_{95}Ti_5$ appeared at 389 °C. The γ-$Fe_{95}Ti_5$ has lower reducibility than the γ-$Fe_{100}Ti_0$. This shows good accordance with the XPS results. The titanium doping inhibited the oxidization ability of the γ-$Fe_{100}Ti_0$. This may lead to the decrease of C-O reaction over the γ-$Fe_{95}Ti_5$ in the SCR reaction.

The reduction peak of $Fe_3O_4 \rightarrow FeO$ process is generally located in the temperature range of 450–500 °C, and that of the $FeO \rightarrow Fe$ process is in the range of 600–700 °C. The wide reduction peaks of $Fe_3O_4 \rightarrow FeO \rightarrow Fe$ process were intercepted and peak-separating fitted using the Gauss method (Fig. 3**S**). Peak 1 and peak 1' were attributed to the reduction peaks of $Fe_3O_4 \rightarrow FeO$ for the γ-$Fe_{100}Ti_0$ and γ-$Fe_{95}Ti_5$ respectively. Peak 2 and peak 2' were attributed to the reduction of $FeO \rightarrow Fe$. Titanium doping mainly affected the reduction process of $Fe_3O_4 \rightarrow FeO$. Peak 1' and peak 2' shifted to higher temperature compared with peaks 1 and 2, which indicating that the oxidization ability of the γ-$Fe_{95}Ti_5$ was actually low. The high reduction temperature on the γ-$Fe_{95}Ti_5$ indicates the mobility of lattice oxygen was greatly weakened. This can be due to the reduction of electronegativity for iron cations and also the larger ionic radius of Ti^{4+}. The weakening of mobility of lattice oxygen could make a majority of Fe^{3+} species firmly confined in the crystal structure of γ-$Fe_{2-\zeta}Ti_\zeta O_{3+\xi}$. This increased the difficulty for accomplishing the redox process from Fe^{3+} to Fe^{2+}. This will avoid the conversion from γ-Fe_2O_3 to Fe_3O_4 or α-Fe_2O_3, thus, improving the stability of maghemite bulk phase. The TG curve of the γ-$Fe_{95}Ti_5$ shown in Fig. 6 confirms the above statement. The γ-$Fe_{95}Ti_5$ exhibited excellent thermal stability in the SCR temperature range.

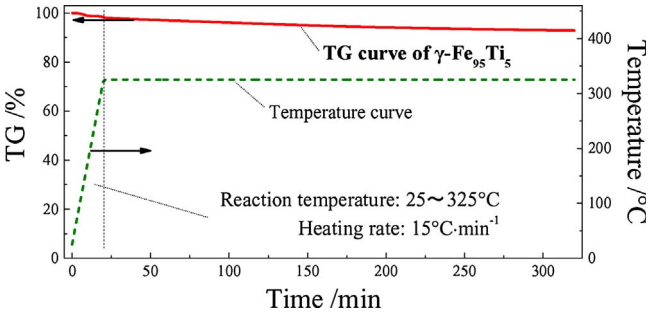

Fig. 6. TG curve of γ-$Fe_{95}Ti_5$ Reaction atmosphere: N_2 (99.99 vol.%); Reaction temperature: 325 °C; Sample weight: 10 ± 0.1 mg; Flow rate: 100 mL·min^{-1}.

3.3.2. Surface acidity

In order to reveal the relative quantity distribution of the surface acid sites over maghemite catalysts, NH_3-TPD experiments were employed on the γ-$Fe_{100}Ti_0$ and γ-$Fe_{95}Ti_5$ (Fig. 5b) [29]. The NH_3 desorption peaks appeared lower than 100 °C were mostly due to physical adsorption. NH_3 desorption in the range of 100 − 250 °C were attributed to the weak acidity, whereas the desorption peaks in the range of 250–500 °C were attributed to the strong acidity. Both weak and strong acidity contain Lewis and Brönsted acid sites.

The γ-$Fe_{95}Ti_5$ presented more than twice of desorption peak areas than the γ-$Fe_{100}Ti_0$. The 4 NH_3 desorption peaks (b") on the γ-$Fe_{100}Ti_0$ appeared at 250–500 °C, indicating that there was rarely weak acidity on the catalyst surface. For the γ-$Fe_{95}Ti_5$, there are 2 distinct NH_3 desorption peaks (a') in the range of 100–250 °C and several NH_3 desorption peaks (a") in the range of 250–500 °C. The a' and a" correspond

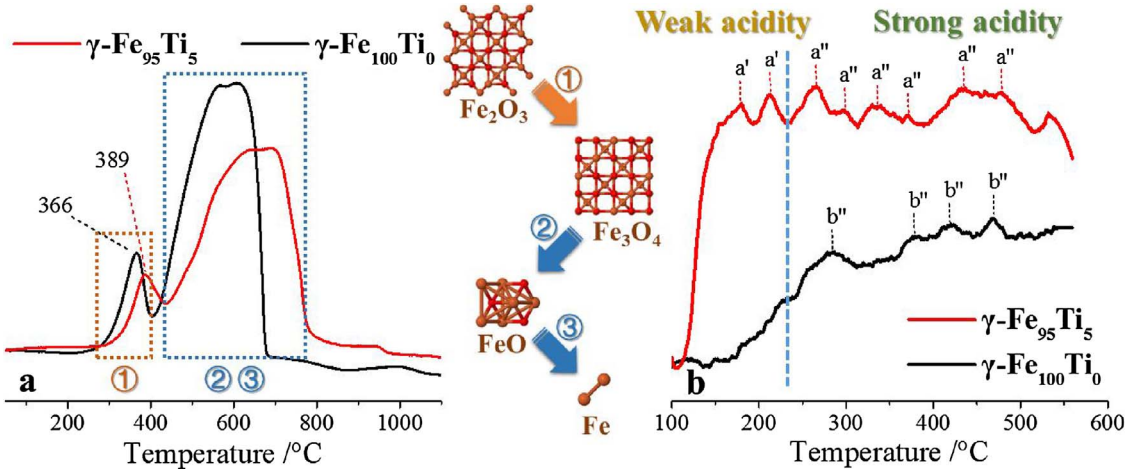

Fig. 5. H_2-TPR (a) and NH_3-TPD (b) profiles over maghemite catalysts.

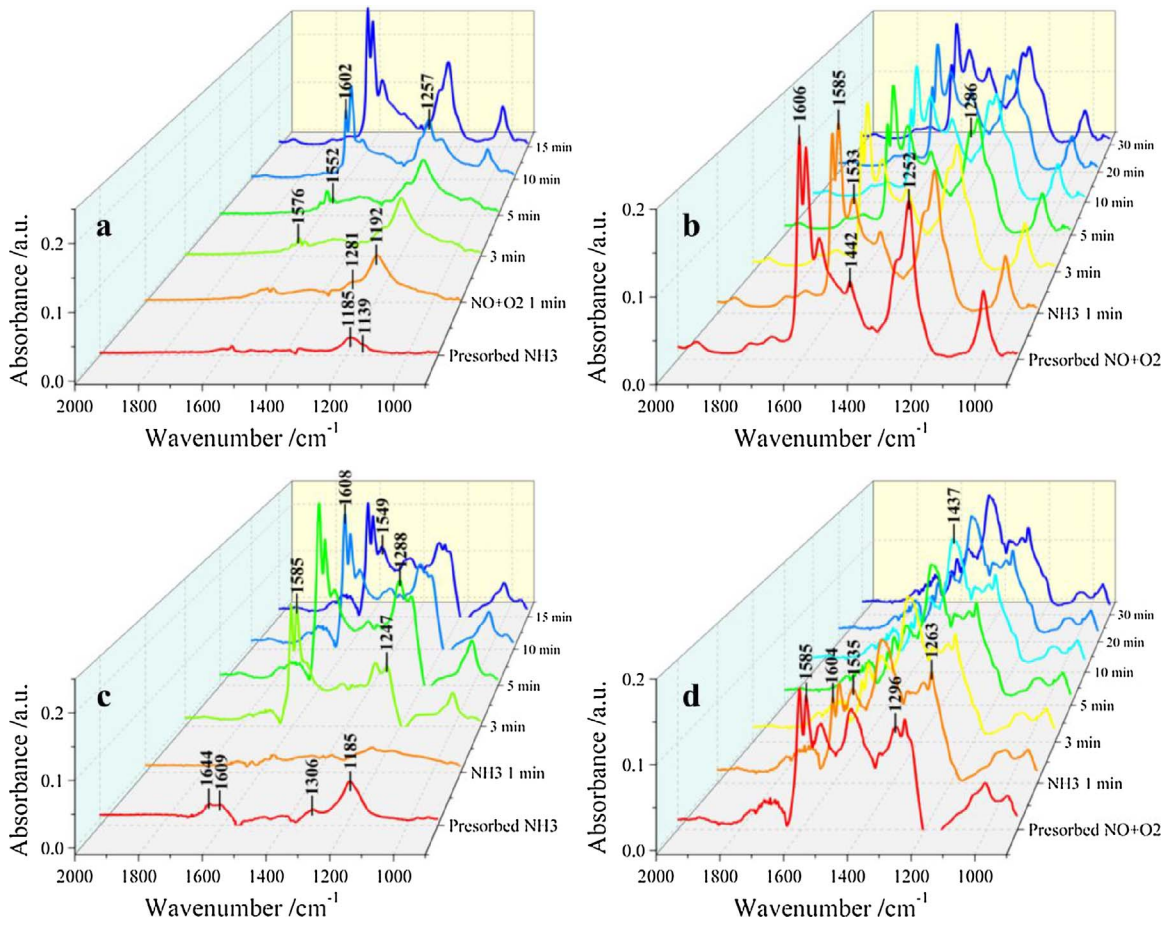

Fig. 7. DRIFT spectra taken at 200 °C upon passing NO + O_2 over NH_3 presorbed: (a) γ-$Fe_{100}Ti_0$; (b) γ-$Fe_{95}Ti_5$. DRIFT spectra taken at 200 °C upon passing NH_3 over NO + O_2 presorbed: (c) γ-$Fe_{100}Ti_0$; (d) γ-$Fe_{95}Ti_5$.

to the weak and strong acidity respectively. These acid sites ensured the γ-$Fe_{95}Ti_5$ to obtain enough adsorbed NH_3 to fulfill the SCR cycle.

The weak acidity is related to the formation of cations vacancies on the surface of the γ-$Fe_{2-\xi}Ti_\xi O_{3+\xi}$. The increase of strong acidity is due to the presence of Ti^{4+} on the catalyst surface. Overall, the doping of titanium can maximize the amount of both weak and strong acidity.

3.3.3. *In situ DRIFTS study*

Fig. 4**S** shows in situ DRIFT spectra of the adsorption of NH_3 on the γ-$Fe_{100}Ti_0$ and γ-$Fe_{95}Ti_5$ at 150 °C. Peak centered at 1185 cm^{-1} and a shoulder at 1139 cm^{-1} were obtained on the γ-$Fe_{100}Ti_0$. They can be attributed to the Lewis acid sites. While two more peaks at 1644 and 1609 cm^{-1} can be obtained from the spectra of the γ-$Fe_{95}Ti_5$. These two peaks can be assigned to the Lewis acid sites. Peak centered at 1306 cm^{-1} can be attributed to Brönsted acid sites. The results indicate that Brönsted acid sites increases in quantity and new Lewis acid sites formed on the catalyst surface after Ti doping. The amount of both Lewis and Brönsted acid sites improved. This is consistent with the significant increase in the amount of both weak and strong acidity in the previous discussions.

The sequential DRIFTS experiments are carried out at 200 °C for the catalysts (Fig. 7a). When NO and O_2 were introduced into the NH_3 pretreated γ-$Fe_{100}Ti_0$, the intensity of Lewis acid sites weakened and vanished more than 5 min. Whereas for the γ-$Fe_{95}Ti_5$ under the same process, both the Lewis and Brönsted acid sites vanished only in 1 min. This indicates that the adsorbed ammonia species of the γ-$Fe_{95}Ti_5$ react with NO_x much faster than that of the γ-$Fe_{100}Ti_0$.

Fig. 7b and d shows the results of the two catalyst when we reversed the gas order. After NH_3 were introduced into NO and O_2 pretreated the γ-$Fe_{100}Ti_0$ at 200 °C, the bands corresponding to adsorbed nitrite gradually decreased (at 1606 cm^{-1}). It suggests that adsorbed nitrogen oxide on the γ-$Fe_{100}Ti_0$ can react with ammonia. Therefore, both the L-H mechanism and the E-R mechanism account for the SCR over the γ-$Fe_{100}Ti_0$. As for the γ-$Fe_{95}Ti_5$, monodentate nitrite (1604, 1585, 1535 and 1263 cm^{-1}) diminished significantly. It implies that the reaction between ammonia and adsorbed nitrogen oxides on the γ-$Fe_{95}Ti_5$ are considerable. Therefore, the L-H mechanism on the γ-$Fe_{95}Ti_5$ could contribute more to the SCR reaction.

3.4. *Kinetic study*

3.4.1. *Steady state kinetics*

In order to identify the contribution of L-H mechanism, E-R mechanism, and C-O reaction to the SCR reaction. Experiments for quantitative kinetics study were performed (Fig. 5S and Fig. 6S). The rates of the NH_3 conversion, NO_x conversion, N_2 formation, N_2O formation, and the C-O reaction during NO reduction on the γ-$Fe_{100}Ti_0$ with gaseous NO concentration were far different from that on the γ-$Fe_{95}Ti_5$. The rates of NO_x conversion, N_2 formation, and N_2O formation on the γ-$Fe_{100}Ti_0$ and γ-$Fe_{95}Ti_5$ increased as increasing the NO concentration. The curve fitting shows that the reaction order of NH_3 conversion with respect to gaseous NO concentration was nearly zero, while the reaction orders of NO_x conversion, N_2 formation, N_2O formation, and NH_3 conversion with respect to gaseous NO concentration were all in the range of 0–1 [19]. The rates of the C-O reaction on the γ-$Fe_{100}Ti_0$ and γ-$Fe_{95}Ti_5$ increased with increasing the temperature. Meanwhile, the rates of the C-O reaction of these two catalysts decreased with increasing the NO concentration. It suggests that reaction orders of the C-

Table 2
The rate constants of the SCR reaction through the E-R mechanism ($k_{SCR\text{-}ER}$) and the L-H mechanism ($k_{SCR\text{-}LH}$), and the rate of the C-O reaction ($\delta_{C\text{-}O}$) with [NH_3] = [NO] = 500 ppm/ μmol·g^{-1}·min^{-1}.

	Temperature/°C	$\delta_{SCR}=K_{SCR\text{-}ER}[NO_{(g)}] + K_{SCR\text{-}LH}$			$\delta_{C\text{-}O}$ ([NH_3] = [NO] = 500 ppm)
		$k_{SCR\text{-}LH}$	$k_{SCR\text{-}ER}/10^6$	R^2	
γ-$Fe_{100}Ti_0$	200	1.3261	0.0038	0.9990	0
	250	3.9155	0.0124	0.9912	1.095
	300	6.8196	0.0316	0.9813	11.501
	350	14.438	0.0328	0.9752	73.458
	400	19.766	0.0512	0.9749	335.926
γ-$Fe_{95}Ti_5$	200	0.4742	0.0369	0.9922	0
	250	9.1843	0.0679	0.9991	0
	300	11.089	0.1209	0.9939	2.329
	350	22.351	0.1511	0.9974	17.331
	400	35.389	0.1513	0.9921	68.355

O reaction with respect to gaseous NO concentration are less than zero [20,30–33].

The SCR reaction, the NSCR reaction and the C-O reaction all contributed to NH_3 conversion. Therefore, the rate of NH_3 conversion can be described as:

$$\delta_{NH_3}=\delta_{SCR}+\delta_{NSCR}+\delta_{C\text{-}O} \quad (4)$$

where δ_{SCR}, δ_{NSCR}, $\delta_{C\text{-}O}$, and δ_{NH3} were the rates of the SCR reaction (i.e. N_2 formation), the NSCR reaction (i.e. N_2O formation), the C-O reaction, and NH_3 conversion, respectively [34].

The C-O reaction contributed to NO formation, while both the SCR reaction and the NSCR reaction contributed to NO reduction. Therefore, the rate of NO_x conversion (NO_2 discarded) can be described as:

$$\delta_{NO}=\delta_{SCR}+\delta_{NSCR}-\delta_{CO} \quad (5)$$

Therefore, the rate of the C-O reaction can be described as:

$$\delta_{C\text{-}O}=\frac{\delta_{NH_3}-\delta_{NO}}{2} \quad (6)$$

3.4.2. Quantitative reaction mechanism

The kinetic model adopted in this paper was derived through the Eley-Rideal mechanism, the Langmuir-Hinshelwood mechanism, the NSCR reaction and the C-O reaction. All the reaction paths mentioned above have been widely recognized and is suitable for iron based catalysts [35,36]. The conclusions based on this model have been proposed to be used in many complex conditions. The reaction mechanism, construction and derivation of the NH_3-SCR reaction kinetic model over maghemite catalysts are shown in ***supporting information***. According to the derivation, the rate of N_2O formation over maghemite catalysts can be described as:

$$\delta_{NSCR}=\frac{d[N_2O]}{dt}=k_2\frac{k_4[NH_2]}{k_2[NO_{(g)}]+k_5}[NO_{(g)}][Fe^{3+}{=}O]=\frac{k_4[NH_2][Fe^{3+}{=}O]}{1+\frac{k_5}{k_2[NO_{(g)}]}} \quad (7)$$

The rate of the C-O reaction over maghemite catalysts can be described as:

$$\delta_{C\text{-}O}=k_5\frac{k_4[NH_2]}{k_2[NO_{(g)}]+k_5}[Fe^{3+}{=}O]=\frac{k_4[NH_2][Fe^{3+}{=}O]}{\frac{k_2[NO_{(g)}]}{k_5}+1} \quad (8)$$

The rate of N_2 formation over maghemite catalysts can be described as:

$$\delta_{N_2}=\frac{d[N_2]}{dt}|_{L\text{-}H}+\frac{d[N_2]}{dt}|_{E\text{-}R}=k_6[Fe^{2+}\text{-}O\text{-}NO\text{-}NH_3]+k_1[NH_2][NO_{(g)}]$$
$$=k_{SCR\text{-}LH}+k_{SCR\text{-}ER}[NO_{(g)}]$$
$$k_{SCR\text{-}LH}=k_6[Fe^{2+}\text{-}O\text{-}NO\text{-}NH_3]$$
$$k_{SCR\text{-}ER}=k_1[NH_2] \quad (9)$$

where, $k_{SCR\text{-}LH}$ and $k_{SCR\text{-}ER}$ are the rate constants of N_2 formation through the L-H mechanism and the E-R mechanism, respectively.

Hinted by Eq. (7), the rate of N_2O formation did not vary notably with increasing the NO concentration when the value was quite high. This is similar to the phenomenon shown in Figs. 5**S d** and **6S d**. Figs. 5**S e** and **6S e** show that the rate of the C-O reaction obviously decreased with increasing the NO concentration. The slight deviation was related to the competition adsorption between NH_3 and NO_2^- on maghemite catalysts. Therefore, we propose the model can be validated.

Figs. 5**S c** and **6S c** suggest that there is a linear relationship between the rate of N_2 formation and NO concentration. This is consistent with the hint of Eq. (9). The contribution of L-H mechanism to NO reduction can be neglected when the intercept ($k_{SCR\text{-}LH}$) of this linear regression was close to zero. However, the intercepts in Figs. 5**S c** and **6S c** were both much higher than zero, suggesting that the contribution of L-H mechanism to NO reduction should not be neglected. Therefore, the adsorption of NO_x over maghemite catalysts need to be involved in the calculation. According to Eq. (9), the reaction kinetic constants of the SCR reaction through the L-H (i.e. $k_{SCR\text{-}LH}$), E-R ($k_{SCR\text{-}ER}$) and the rates of the C-O are listed in Table 2 and Fig. 8.

The contributions of the NSCR reaction to NH_3 conversion on the γ-$Fe_{100}Ti_0$ and γ-$Fe_{95}Ti_5$ were both minimal at 200 − 400 °C. Most of NH_3 was oxidized by the γ-$Fe_{100}Ti_0$ above 350 °C (Fig. 5**S e**), therefore the SCR activity was mainly related to the C-O reaction. The C-O reaction is restrained with increasing the NO concentration, resulting in the improvement of SCR activity over the γ-$Fe_{100}Ti_0$ and γ-$Fe_{95}Ti_5$ at higher temperatures. Fig. 5**S c** demonstrates that the increase of gaseous NO concentrations from 300 to 700 ppm caused the improvement of SCR activity over the γ-$Fe_{100}Ti_0$ above 350 °C. Similar phenomenon was also found on the γ-$Fe_{95}Ti_5$ in the range of 200 − 400 °C (Fig. 6**S c**).

The adsorption of NH_3 on maghemite catalysts were enhanced obviously after titanium doping. Hinted by Equation 13S, NH_2 concentration on the γ-$Fe_{95}Ti_5$ increases. According to **Equations 11S** and **9**, $k_{SCR\text{-}ER}$ and $k_{SCR\text{-}LH}$ both enhance after increasing the NH_2 concentration on the γ-$Fe_{95}Ti_5$. Fig. 8 demonstrates that $k_{SCR\text{-}ER}$ and $k_{SCR\text{-}LH}$ improve after titanium doping, resulting in an increase of NO reduction rate. As a result, the apparent NO_x conversion of the γ-$Fe_{95}Ti_5$ increased compared to that of the γ-$Fe_{100}Ti_0$. However, the C-O reaction happened on maghemite catalysts higher than 300 °C. $\delta_{C\text{-}O}$ decreases after titanium doping. The NO reduction rate dropped with decreasing the NO concentration, while the C-O reaction rate increased. It suggests that the rate of NO conversion would gradually decrease with the

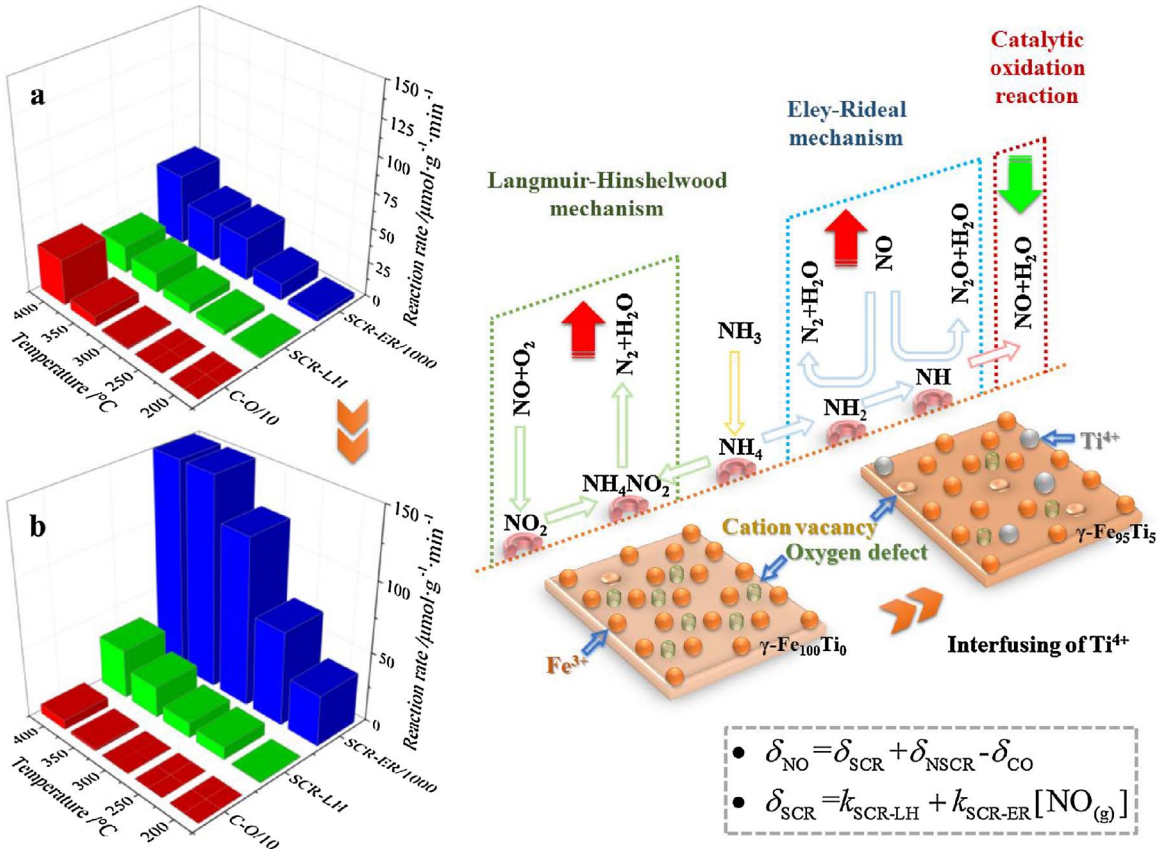

Fig. 8. Quantitative analysis of the SCR reaction path over maghemite catalysts: (a) γ-$Fe_{100}Ti_0$, (b) γ-$Fe_{95}Ti_5$.

reduction of NO over the γ-$Fe_{100}Ti_0$. The rate of the C-O reaction obviously decreased above 300 °C especially at low NO concentration.

Overall, SCR reaction (both E-R and L-H mechanisms), NSCR reaction and C-O reaction are responsible for the NO conversion. The discussed kinetic equations showed an excellent linear relationship between the rate of the SCR reaction and gaseous NO concentration, the intercept and slope of which related to the L-H and E-R mechanisms respectively. The reaction order of the C-O reaction with respect to gaseous NO concentration was less than zero. The titanium doping significantly inhibited the rate of C-O but increase both the rate of L-H and E-R mechanisms. As a result, the SCR activity of maghemite catalyst was improved notably.

4. Conclusions

The trace amount of titanium doping improved the physical and chemical properties of maghemite catalyst significantly by forming solid. Iron and titanium were in the form of Fe^{3+} and Ti^{4+} cations respectively. Lattice oxygen was enriched for maintaining the electrical neutrality of the catalyst. Moreover, the electronegativity of iron cations decreased, mitigating the activity and mobility of Fe^{3+}. These changes brought two important ameliorations: (1) catalyst reducibility decreased; (2) both Lewis and Brönsted acid sites increased. According to the DRIFTS and kinetics studies, L-H and E-R mechanisms both account for the SCR reaction. The reaction rate constants of E-R ($k_{SCR\text{-}ER}$) and L-H mechanisms ($k_{SCR\text{-}LH}$) increased simultaneously, and the reaction rate of the C-O reaction ($\delta_{C\text{-}O}$) decreased.

Acknowledgements

This work was financially supported by the National Key Research and Development Program (2017YFC0210700, 2017YFC021020X), the National Natural Science Foundation of China (21325731, 51576117, 21777081), the Ministry of Environmental Protection of China (201509021, 201509012) and the project funded by China Postdoctoral Science Foundation (2016M601052).

Appendix A. Supplementary data

Supplementary data associated with this article can be found, in the online version, at http://dx.doi.org/10.1016/j.apcatb.2017.09.045.

References

[1] Y. Peng, W. Si, X. Li, J. Luo, J. Li, J. Crittenden, J. Hao, Appl. Catal. B 181 (2016) 692.
[2] Q. Zou, K. Lu, Y. Wu, Y. Yang, Z. Du, M. Hu, Front. Environ. Sci. Eng. 10 (2016) 13.
[3] S. Xiong, J. Weng, Y. Liao, B. Li, S. Zou, Y. Geng, X. Xiao, N. Huang, S. Yang, J. Phys. Chem. C 120 (2016) 15299.
[4] Y. He, M.E. Ford, M. Zhu, Q. Liu, U. Tumuluri, Z. Wu, I.E. Wachs, Appl. Catal. B 193 (2016) 141.
[5] S. Dahlin, M. Nilsson, D. Bäckström, S.L. Bergman, E. Bengtsson, S.L. Bernasek, L.J. Pettersson, Appl. Catal. B 183 (2016) 377.
[6] Y. Peng, W. Si, X. Li, J. Chen, J. Li, J. Crittenden, J. Hao, Environ. Sci. Technol 50 (2016) 9576.
[7] X. Li, J. Li, Y. Peng, H. Chang, T. Zhang, S. Zhao, W. Si, J. Hao, Appl. Catal. B 184 (2016) 246.
[8] D.E. Doronkin, S. Fogel, P. Gabrielsson, J.D. Grunwaldt, S. Dahl, Appl. Catal. B 148–149 (2014) 62.
[9] Y. Peng, J. Li, W. Si, X. Li, W. Shi, J. Luo, J. Fu, J. Crittenden, J. Hao, J. Chem. Eng. 269 (2015) 44.
[10] J. Wang, H. Zhao, G. Haller, Y. Li, Appl. Catal. B 202 (2017) 346.
[11] S. Deng, T. Meng, B. Xu, F. Gao, Y. Ding, L. Yu, Y. Fan, ACS Catal. 6 (2016) 5807.
[12] T. Zhang, R. Qu, W. Su, J. Li, Appl. Catal. B 176–177 (2015) 338.
[13] Y. Peng, Z. Liu, X. Niu, L. Zhou, C. Fu, H. Zhang, J. Li, W. Han, Catal. Commun. 19 (2012) 127.
[14] T. Kohtake, M. Segawa, A. Yamanaka, J. Cryst. Growth (2016).
[15] O. Stefanescu, M. Stefanescu, J. Organomet. Chem. 740 (2013) 50.
[16] A.K. Yadav, C.R. Gautam, P. Singh, J. Alloy. Compd. 672 (2016) 52.

[17] R. Zhang, H.B. Jin, D. Guo, J. Zhang, Z. Zhao, Y. Zhao, J.B. Li, Ceram. Int. 42 (2016) 18764.
[18] N.Y. Topsoe, Science 265 (1994) 1217.
[19] G. Busca, L. Lietti, G. Ramis, F. Berti, Appl. Catal. B 18 (1998) 1.
[20] M.A. Efstathiou, K. Fliatoura, Appl. Catal. B 6 (1995) 35.
[21] J. Svachula, N. Ferlazzo, P. Forzatti, E. Tronconi, Ind. Eng. Chem. Res. 32 (1993) 1053.
[22] G. Tuenter, W.F. Leeuwen, L.J.M. Snepvangers, Ind. Eng. Chem. Res. 25 (1986) 633.
[23] D. Meng, W. Zhan, Y. Guo, Y. Guo, L. Wang, G. Lu, ACS Catal. 5 (2015) 5973.
[24] W. Shan, F. Liu, H. He, X. Shi, C. Zhang, Chem. Commun. 47 (2011) 8046.
[25] L.J. France, Q. Yang, W. Li, Z. Chen, J. Guang, D. Guo, L. Wang, X. Li, Appl. Catal. B 206 (2017) 203.
[26] H. Ning, H. Yan, Z. Gao, X. Wei, M.J. Reece, Ceram. Int. 39 (2013) 7669.
[27] Y. Peng, W. Si, J. Luo, W. Su, H. Chang, J. Li, J. Hao, J. Crittenden, Environ. Sci. Technol. 50 (2016) 6442.
[28] J.S. Hardy, J.W. Templeton, D.J. Edwards, Z. Lu, J.W. Stevenson, J. Power Sources 198 (2012) 76–82.
[29] M. Mhamdi, S. Khaddar-Zine, A. Ghorbel, Appl. Catal. A 357 (2009) 42.
[30] S. Xiong, Y. Liao, X. Xiao, H. Dang, S. Yang, J. Phys. Chem. C 119 (2015) 4180.
[31] S. Xiong, Y. Liao, X. Xiao, H. Dang, S. Yang, Catal. Sci. Technol. 5 (2015) 2132.
[32] S. Yang, Y. Liao, S. Xiong, F. Qi, H. Dang, X. Xiao, J. Li, J. Phys. Chem. C 118 (2014) 21500.
[33] S. Yang, S. Xiong, Y. Liao, X. Xiao, F. Qi, Y. Peng, Y. Fu, W. Shan, J. Li, Environ. Sci. Technol. 48 (2014) 10354.
[34] S. Yang, F. Qi, Y. Liao, S. Xiong, Y. Lan, Y. Fu, W. Shan, J. Li, Ind. Eng. Chem. Res. 53 (2014) 5810.
[35] J. Ma, H. He, F. Liu, Appl. Catal. B 179 (2015) 21.
[36] Q. Dai, W. Wang, X. Wang, G. Lu, Appl. Catal. B 203 (2017) 31.